

Vacuum Annealing of Nanocrystalline WC Powders

A. S. Kurlov and A. I. Gusev

*Institute of Solid State Chemistry, Ural Branch, Russian Academy of Sciences,
Pervomaiskaya ul. 91, Yekaterinburg, 620990 Russia*

e-mail: kurlov@ihim.uran.ru

Received November 24, 2011

Abstract—The effect of vacuum annealing temperature on the chemical and phase compositions, particle size, and lattice strain of nanocrystalline tungsten carbide (WC) powders with a particle size from 20 to 60 nm has been studied by X-ray diffraction and electron microscopy. The results demonstrate that vacuum annealing of WC nanopowders at $t_{\text{ann}} \leq 1400^\circ\text{C}$ is accompanied by a marked decrease in carbon content and changes in phase composition due to carbon desorption from the surface of the powder as a result of the interaction of carbon with oxygen impurities. In addition, annealing leads to an increase in particle size due to coalescence of aggregated nanoparticles and reduces the lattice strain of the powder.

DOI: 10.1134/S0020168512060088

INTRODUCTION

Currently, the use of nanocrystalline tungsten carbide (WC) powders is regarded as the most promising approach to the fabrication of nanostructured hard alloys with a reduced sintering temperature and enhanced hardness, strength, and fracture toughness [1, 2].

Many processes for the preparation of nanocrystalline WC powders have been proposed to date [3, 4]. There is particular interest in high-energy milling of microcrystalline tungsten carbide (WC) powder [5], which is a “top-down” nanotechnology, and in plasma synthesis from a tungsten oxide and hydrocarbon [6], which is a “bottom-up” nanotechnology.

WC powders are most widely used in the fabrication of hard alloys, the most widespread of which are WC–Co alloys. The highest sintering temperature of microcrystalline WC–Co alloys in conventional processes in vacuum or under a protective or inert atmosphere is 1380 to 1420°C. As shown in previous studies concerned with the oxidation of WC powder [7, 8], a decrease in WC powder particle size is accompanied by a reduction in oxidation onset temperature and increase in oxidation rate [7, 8]. It is, therefore, important to assess the thermal stability of the size and composition of WC nanoparticles at temperatures of up to 1400°C.

The purpose of this work was to examine the temperature effect on the phase composition and size of tungsten carbide (WC) nanoparticles vacuum-annealed at temperatures from 400 to 1400°C.

EXPERIMENTAL

In our vacuum annealing experiments, we used three WC powders differing in particle size, which

were stored in air: microcrystalline powder manufactured at the Kirovgrad Hard Alloys Plant (OAO KZTS, Kirovgrad, Russia), with an average particle size of 9 μm , which will be referred to as WC(micro); nanocrystalline powder with an average particle size of 20 nm, produced by grinding the WC(micro) powder in a Retsch PM 200 planetary ball mill (the milling conditions were similar to those described previously [5, 9, 10]), WC(mill); and nanocrystalline powder with an average particle size of 60 nm synthesized at OAO VNIETO (Moscow, Russia) through a plasma process using tungsten(III) oxide (WO_3) and propane (C_3H_8), which were reacted in a low-temperature hydrogen plasma flow, followed by thermochemical processing (the synthesis procedure was similar to that described in Tsvetkov and Panfilov [6]), WC(plasma). In addition, we annealed a mixture of the WC(mill) nanopowder and 2 wt % MT-900 carbon black (the mixture will be referred to as WC(mill) + C).

Loose WC powders (2–3 g) were annealed in a vacuum of 0.0013 Pa (10^{-5} mm Hg) in an SShV-1.2.5/25I1 laboratory furnace with tungsten lining and heaters. The annealing schedule was as follows: slow (1–2 h, depending on the highest annealing temperature) heating to t_{ann} , holding at t_{ann} for 1 h, and furnace cooling of the powder. The annealing temperatures were 400, 600, 800, 1000, 1200, and 1400°C. In each annealing experiment, only the as-prepared WC powders were used.

The phase composition of the WC powders before and after annealing was determined by X-ray diffraction (XRD) in the angular range $2\theta = 30^\circ\text{--}125^\circ$ with a scan step of 0.03° and a counting time per data point of 2 s (DRON-UM1 diffractometer, $\text{CuK}_{\alpha_{1,2}}$ radiation) XRD patterns were analyzed numerically using Philips Analytical X'Pert Plus (Version 1.0) software.

The particle size distributions in the WC powders were assessed using a Horiba Partica LA-950V2 laser diffraction particle size analyzer. Prior to measurements, the powder to be analyzed was suspended in water. The average size of the powder particles was also evaluated from diffraction data and by scanning electron microscopy (SEM) on a JEOL JSM-6390LA. In addition, the crystallite size D and lattice strain ε of the WC(mill) and WC(plasma) nanocrystalline powders were determined from the width of XRD line profiles. To a first approximation, the average crystallite size thus determined can be regarded as the average particle size D of the nanopowders.

The WC powders were analyzed for total carbon C_{total} and free (uncombined) carbon C_{free} on a Metavak-CS-30 analyzer. Oxygen impurities were determined by a carrier gas method with a Coulomatic-O analyzer and by energy-dispersive X-ray (EDX) analysis on a JEOL JSM-6390LA electron microscope equipped with a JED-2300 spectrometer system. Adsorbed water was determined from the weight loss of a powder sample calcined for 1 h in a vacuum of 1×10^{-4} Pa at 400°C. Spectral analyses were carried out on a PerkinElmer SCIEX-ELAN 9000 mass spectrometer.

RESULTS AND DISCUSSION

The effect of vacuum annealing on the WC(mill) and WC(plasma) nanocrystalline powders was studied in comparison with the WC(micro) microcrystalline powder. According to spectral analysis data, the WC powders before vacuum annealing were similar in impurity content: within 0.1 wt % Na and within 0.01 wt % Fe, Ni, Mo, and Sn. The content of other metallic impurities did not exceed 0.005 wt %. The adsorbed water content of the WC(micro), WC(mill), and WC(plasma) powders before vacuum annealing was 0.1, 1.0, and 0.9 wt %, respectively. The three WC powders were analyzed chemically and characterized by particle size measurements.

Figure 1 shows XRD patterns of the WC(micro), WC(mill), and WC(plasma) powders before vacuum annealing and the WC(micro) powder vacuum-annealed at 1200°C. The as-prepared WC(micro) microcrystalline powder contained, in addition to the higher tungsten carbide WC (hexagonal structure, sp. gr. $P\bar{6}m2$), ≈ 2 wt % W_2C , the lower tungsten carbide (hexagonal structure, sp. gr. $P6_3/mmc$) (Fig. 1, scan 1). The WC(mill) nanopowder was prepared by milling the microcrystalline powder, so it also contained a small amount of W_2C (Fig. 1, scan 3). The as-prepared WC(plasma) plasma-synthesized nanopowder (Fig. 1, scan 4) consisted only of the higher tungsten carbide WC.

Note that impurity phases in the WC nanopowders were rather difficult to detect by XRD (Fig. 1, scans 3, 4) because even reflections from the major phase WC

were relatively broad, so neighboring reflections in the angular range $2\theta > 60^\circ$ overlapped and merged. Analysis of the broadening of the diffraction peaks from the nanopowders showed that it was due to both the small particle size, D , and lattice strain, ε . D and ε were evaluated from the width of XRD line profiles by a procedure described elsewhere [3, 11, 12]. We obtained $D = 20 \pm 10$ nm and $\varepsilon = 0.83 \pm 0.05\%$ for the WC(mill) powder and $D = 60 \pm 10$ nm and $\varepsilon = 0.43 \pm 0.05\%$ for the WC(plasma) powder. The average size of aggregated particles, D_{aggr} , evaluated by laser diffraction on the Horiba Partica LA-950V2 (Fig. 2) was almost one order of magnitude greater than the average crystallite size D of the WC nanopowders. This was due to the formation of large aggregates of nanoparticles. The SEM micrographs in Fig. 3 indicate that the particle size of the WC(mill) and WC(plasma) nanopowders differs little from the average crystallite size, but the nanoparticles indeed form large aggregates, up to several hundred nanometers in size. In the WC(micro) powder, the average particle size is 9 μm according to both laser diffraction (Fig. 2, curve 1) and electron microscopy (Fig. 3a) data, which are in good agreement. The narrow diffraction peaks of this powder (Fig. 1, scan 1) indicate that it consists of large particles and is free of lattice strain.

The specific surface area of powder can be found as $S = 6/\rho D$ [3], where ρ is the density of the material and D is the average particle size. The density of WC is $\rho = 15.67$ g/cm³. From this value and the above average particle sizes, we find that the S of the WC(micro), WC(mill), and WC(plasma) powders before vacuum annealing was 0.04, 19.2, and 6.4 m²/g. The $S = 6.4$ m²/g obtained for the WC(plasma) powder is in reasonable agreement with the $S = 6.0$ – 9.5 m²/g inferred from BET measurements.

Note that the WC(micro) powder, which had the smallest specific surface area, had the lowest adsorbed water content, 0.1 wt %, whereas the as-prepared WC(mill) nanopowder, which had the largest specific surface area, contained the largest percentage of adsorbed water, 1.0 wt %.

The chemical and phase compositions and other characteristics of the as-prepared and annealed WC powders are presented in the table. According to chemical analysis data for total and free carbon, the as-prepared powders contained 6.14 ± 0.15 wt % C_{total} and 0.15 ± 0.10 wt % C_{free} (table), which corresponds to the tungsten carbide WC. It is worth noting that the unannealed WC(mill) nanopowder, produced by milling the WC(micro) powder, contained more C_{total} by ≈ 0.3 wt % compared to the WC(micro) powder. Almost all of this difference is accounted for by free carbon, which was essentially missing in the WC(micro) powder before vacuum annealing. This seems to be related to the powder preparation process.

The oxygen content of the WC(micro), WC(mill), and WC(plasma) powders before vacuum annealing

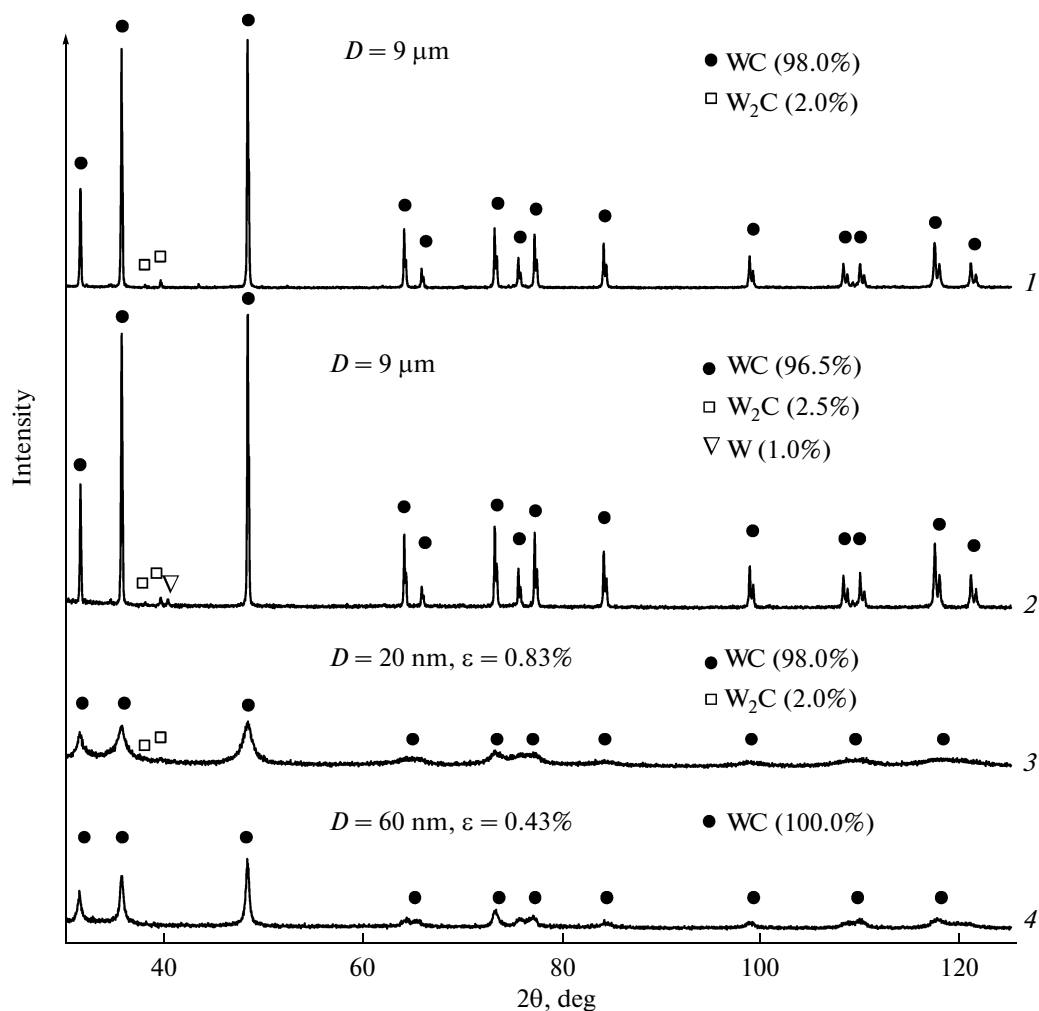


Fig. 1. XRD patterns of WC powders: (1) as-prepared WC(micro) microcrystalline powder, average particle size of $9 \pm 1 \mu\text{m}$; (2) WC(micro) powder vacuum-annealed at 1200°C ; (3) as-prepared WC(mill) nanocrystalline powder, $D = 20 \pm 10 \text{ nm}$; (4) as-prepared WC(plasma) nanocrystalline powder, $D = 60 \pm 10 \text{ nm}$.

was 0.11, 0.91, and 1.23 wt %, respectively, according to chemical analysis data and 0.12 ± 0.05 , 1.52 ± 0.05 , and 1.80 ± 0.1 wt % according to EDX analysis data. After annealing, no EDX analysis was performed because, when exposed to air, the annealed WC powders reabsorbed water and oxygen, and their concentrations returned to their original level in a few hours.

Vacuum annealing of the WC(micro) powder. The WC(micro) powder was vacuum-annealed at 1200°C . Chemical analysis and XRD data showed that annealing reduced the carbon content of the powder, but without significant changes in its phase composition. As seen in Fig. 1, the XRD patterns of the WC(micro) powder before and after annealing (scans 1, 2) are almost identical. The only distinction is that the XRD pattern of the annealed powder contains one, weak reflection from tungsten. Quantitative phase analysis showed that annealing at 1200°C reduced the content of the major phase (WC) in the WC(micro) powder by

1.5 wt % and increased the W_2C content by 0.5 wt %. In addition, it produced ≈ 1.0 wt % W (table). According to chemical analysis data, the annealing reduced the carbon content of the WC(micro) powder by no more than ≈ 0.01 wt %.

Vacuum annealing of the WC(mill) powder and WC(mill) + C mixture. After vacuum annealing of the WC(mill) nanopowder at 400 and 600°C , no changes in its XRD pattern were detected. At the same time, chemical analysis showed that raising t_{ann} to 600°C reduced the carbon content of the powder by almost 1 wt % and that the annealed powder contained free carbon (table). Diffraction peak broadening analysis indicated that annealing at 600°C had no effect on the particle size of the powder but reduced the lattice strain from 0.83 to 0.64%. Annealing of the WC(mill) nanopowder at 800°C reduced the total carbon content by 1.5 wt % (relative to the original level) and the free carbon content to zero. After this anneal, the

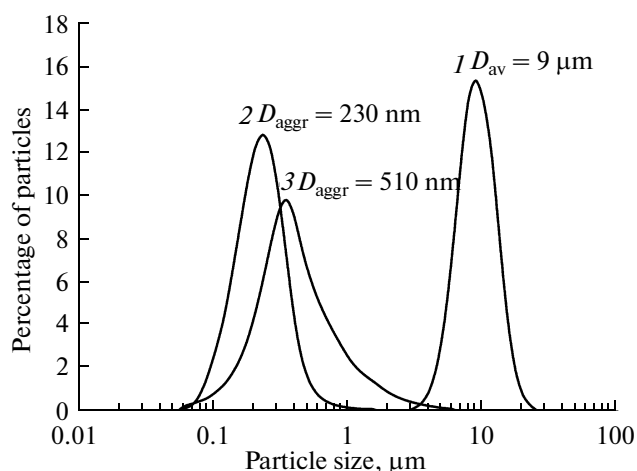


Fig. 2. Particle size distributions (laser diffraction data) in the WC powders before annealing: (1) WC(micro), $D_{av} = 9 \mu\text{m}$; (2) WC(mill), $D_{aggr} = 230 \text{ nm}$; (3) WC(plasma), $D_{aggr} = 510 \text{ nm}$.

XRD pattern of the powder (Fig. 4, scan 2) showed sharp peaks of metallic tungsten (sp. gr. $Im\bar{3}m$). The diffraction peaks of WC became narrower, which corresponded to an increase in average particle size to 30 nm and a decrease in lattice strain to 0.6%. W_2C was missing, even though the unannealed WC(micro) powder, which was milled to produce the WC(mill) powder, contained 2 wt % W_2C . Annealing of the WC(mill) powder at 800 and 1000°C yielded almost identical phase compositions, which only differed in WC to W ratio. Raising the annealing temperature to 1000°C was accompanied by a decrease in the total carbon content and an increase in the W content of the WC(mill) nanopowder. In addition, the WC particle size increased to 50 nm. After annealing at 1200°C, the WC(mill) powder contained, in addition to WC and W, about 7 wt % W_2C (Fig. 4, scan 3). As t_{ann} was raised to 1400°C, the W_2C content increased to ≈ 36 wt %, whereas W disappeared (Fig. 4, scan 4). Annealing at 1400°C reduced the total carbon content of the WC(mill) powder by about 1.5 wt % relative to the original level, increased the average particle size by four times (to 80 nm), and reduced the lattice strain to 0.26%.

To prevent annealing-induced decarburization of the WC(mill) powder and maintain its phase purity, 2 wt % carbon (MT-900 carbon black) was added to the as-prepared powder. The WC(mill) + C mixture was vacuum-annealed at 1200°C, like the WC(mill) powder with no carbon additions. The XRD pattern of the annealed WC(mill) + C powder mixture showed rather narrow reflections, which were due to only one phase: the higher tungsten carbide WC (Fig. 4, scan 5). Diffraction peak broadening analysis indicated that the anneal increased the average particle size to 110 nm and reduced the lattice strain to almost zero (0.05%). According to chemical analysis data, the

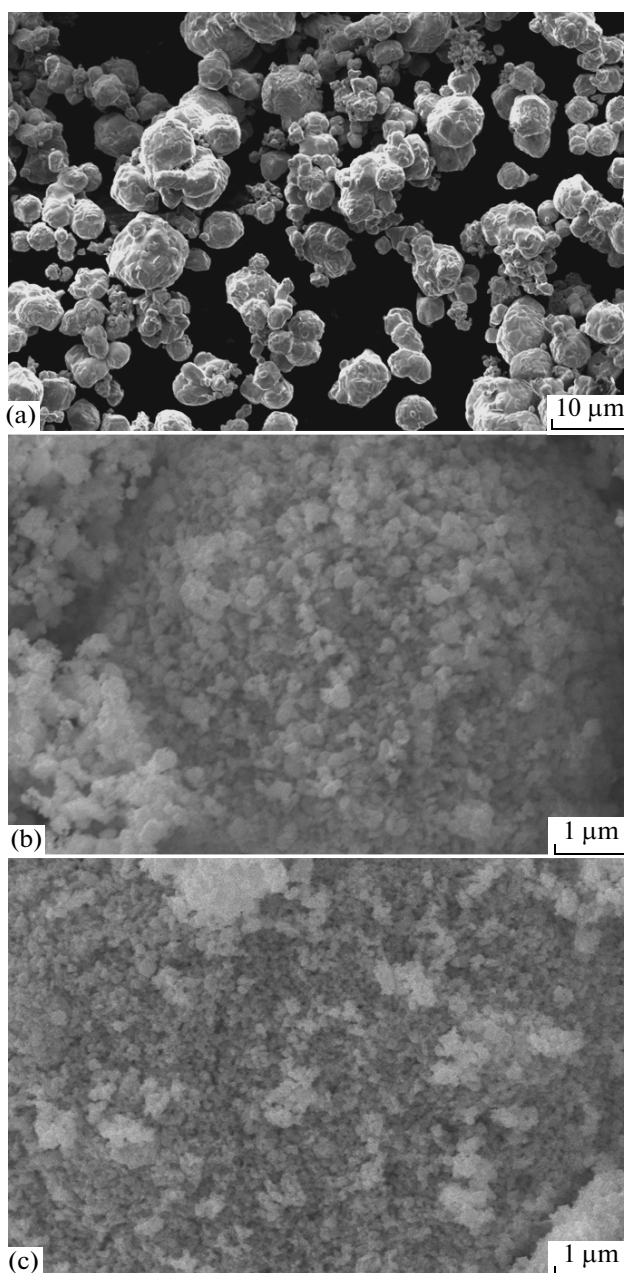


Fig. 3. SEM micrographs of the tungsten carbide powders before vacuum annealing: (a) WC(micro), (b) WC(mill), (c) WC(plasma).

annealed WC(mill) + C mixture contained 6.28 wt % total carbon and 1.28 wt % free carbon.

SEM examination showed that vacuum annealing of the WC(mill) powder at $t_{ann} \leq 800^\circ\text{C}$ had little effect on the particle size and shape (Fig. 5a), which remained stable. Annealing at 1200°C and above produced coarser particles (Figs. 5b, 5c), which resulted from the coalescence of aggregated nanoparticles. According to SEM data, the WC(mill) + C mixture annealed at 1200°C contained, in addition to fine parti-

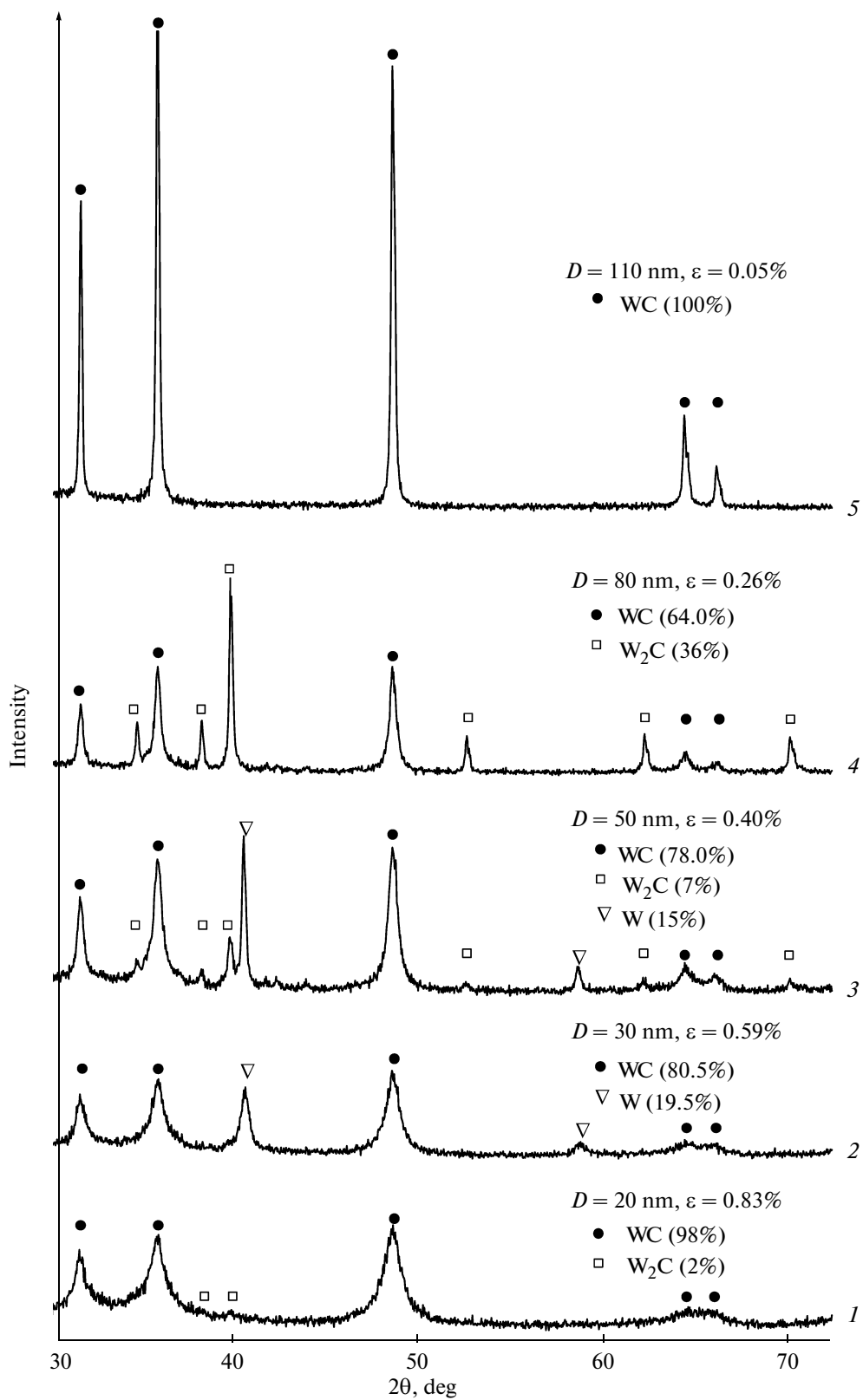


Fig. 4. XRD patterns of the (1) as-prepared and (2–4) vacuum-annealed WC(mill) nanopowder and (5) vacuum-annealed WC(mill) + 2 wt % carbon powder mixture; annealing temperature of (2) 800, (3, 5) 1200, and (4) 1400°C.

Chemical and phase compositions, average particle size D , specific surface area S , and lattice strain ε of as-prepared and vacuum-annealed WC powders

Powder	$t_{\text{ann}} \pm 10$, °C	$D \pm 10$, nm	S , m ² /g	$\varepsilon \pm 0.05$, %	Phase composition ± 0.1 wt %			Chemical composition ± 0.05 wt %		
					WC	W	W ₂ C	C _{total}	C _{free}	O ^{**}
WC(micro)	—	9000 \pm 1000*	0.04	—	98.0	0	2.0	6.00	0.05	0.11
WC(mill)		20	19.2	0.83	98.0	0	2.0	6.27	0.24	0.91
WC(plasma)		60	6.4	0.43	100.0	0	0	6.14	0.18	1.23
WC(mill)	400	20	19.2	0.69	98.0	0	2.0	5.89	0.70	—
WC(plasma)		60	6.4	0.42	100.0	0	0	5.86	0.14	—
WC(mill)	600	20	19.2	0.64	98.0	0	2.0	5.31	0.58	—
WC(plasma)		60	6.4	0.36	100.0	0	0	6.09	0.16	—
WC(mill)	800	30	12.8	0.59	80.5	19.5	0	5.15	Not detected	—
WC(plasma)		70	5.5	0.38	79.0	21.0	0	5.16	Not detected	—
WC(mill)	1000	50	7.7	0.60	77.5	22.5	0	4.84	Not detected	—
WC(plasma)		80	4.8	0.39	80.5	19.5	0	5.07	Not detected	—
WC(micro)	1200	9000 \pm 1000*	0.04	—	96.5	1.0	2.5	5.99	Not detected	—
WC(mill)		50	7.7	0.40	78.0	15.0	7.0	4.82	Not detected	—
WC(mill) + C		110	3.5	0.05	100.0	0	0	6.28	1.28	—
WC(plasma)		80	4.8	0.35	79.5	20.5	0	4.96	Not detected	—
WC(mill)	1400	80	4.8	0.26	64.0	0	36.0	4.83	Not detected	—
WC(plasma)		80	4.8	0.18	65.0	2.0	33.0	4.66	Not detected	—

*The average particle size of the WC(micro) powder was found from the particle size distribution (Fig. 2, curve 1) obtained by laser diffraction.

**Oxygen in the WC powders was determined only before annealing.

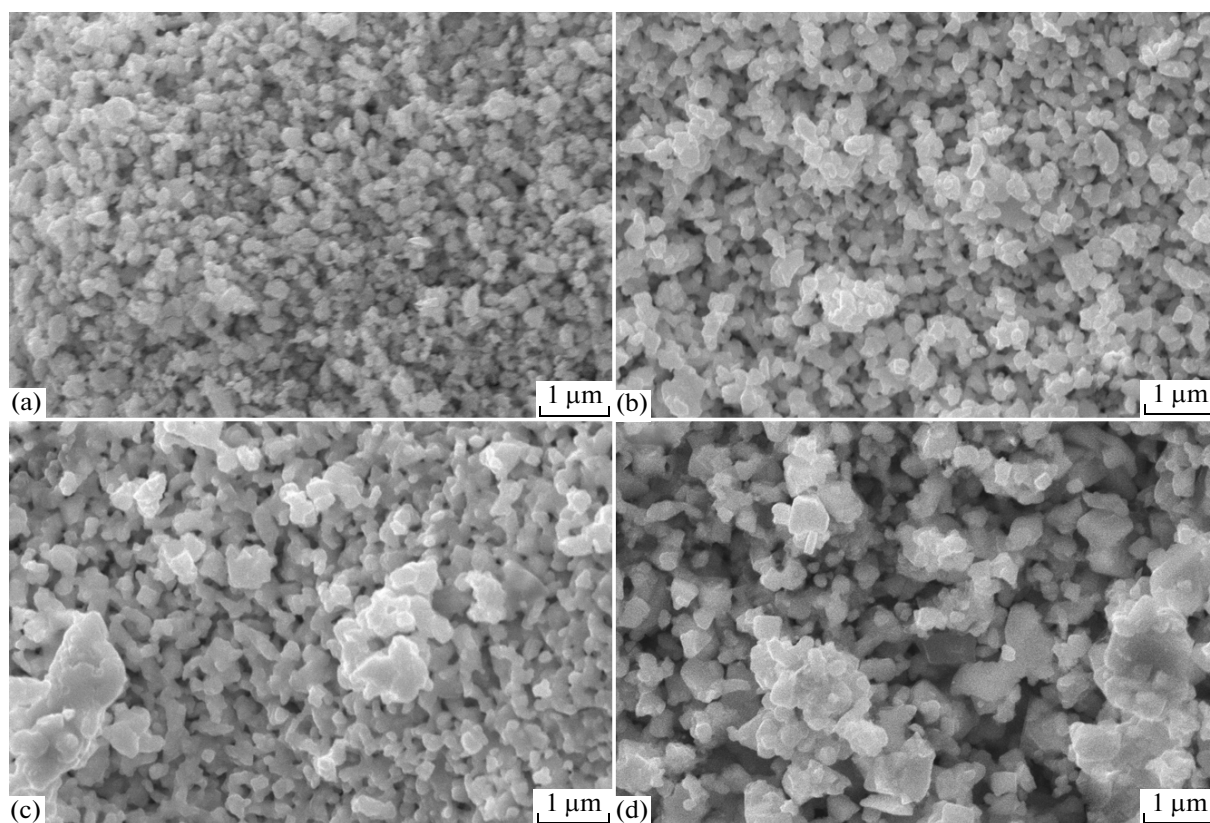


Fig. 5. SEM micrographs of the WC(mill) nanopowder vacuum-annealed at 800 (a), 1200 (b), and 1400°C (c) and the WC(mill) + 2 wt % carbon powder mixture vacuum-annealed at 1200°C (d).

cles ≈ 200 nm in size, large, well-faceted particles up to 1.0–1.5 μm in size (Fig. 5d).

Thus, the addition of carbon allows WC nanopowder to retain its phase purity during annealing but leads to marked particle growth even at moderate annealing temperatures.

Vacuum annealing of the WC(plasma) powder. According to XRD data, vacuum annealing at 400 and 600°C produced no changes in the phase composition, average particle size, or lattice strain of the WC(plasma) nanopowder. Compositional stability of this powder was also evidenced by chemical analysis data, which indicated that the total carbon content was sufficient for WC formation and that the powder contained free carbon. At the same time, annealing at 800°C slightly increased the particle size, to 70 nm, and had a significant effect on the phase composition of the powder: in addition to the major phase WC, it contained about 21 wt % metallic tungsten (Fig. 6, scan 2). Chemical analysis data showed that the total carbon content decreased by about 1 wt % and that the free carbon content dropped to zero. As t_{ann} was raised from 800 to 1200°C, the particle size of the carbide phase slightly increased (to 80 nm) and the lattice strain and total carbon content slightly decreased, which, however, had little effect on the phase composition of the powder (79.5 wt % WC and 20.5 wt % W).

Significant changes were only detected after annealing of the WC(plasma) powder at 1400°C (Fig. 6, scan 4): the powder contained ≈ 33 wt % W_2C , whereas the tungsten content sharply dropped, to ≈ 2 wt % (the presence of tungsten was only evidenced by a weak reflection at $2\theta = 40.27^\circ$). Diffraction peak broadening analysis indicated that the anneal increased the particle size by 20 nm and reduced the lattice strain by almost a factor of 2 relative to the as-prepared powder. According to chemical analysis data, the anneal reduced the total carbon content by about 1.5% relative to the as-prepared WC(plasma) powder.

SEM examination showed that vacuum annealing had little effect on the shape of the WC(plasma) powder particles but slightly increased their size (Fig. 7), in agreement with the above diffraction data. The annealing-induced increase in the particle size of the WC(plasma) powder was less significant than that of the WC(mill) powder, whose particle size after annealing at 1400°C was four times that of the as-prepared powder. The WC(plasma) powder particles were rounded in shape both before and after annealing: at least, SEM examination failed to detect any aggregated particles similar to those resulting from sintering in the annealed WC(mill) powder. The WC(plasma) nanoparticles were already highly aggregated before annealing. Even after annealing at 1400°C—the tem-

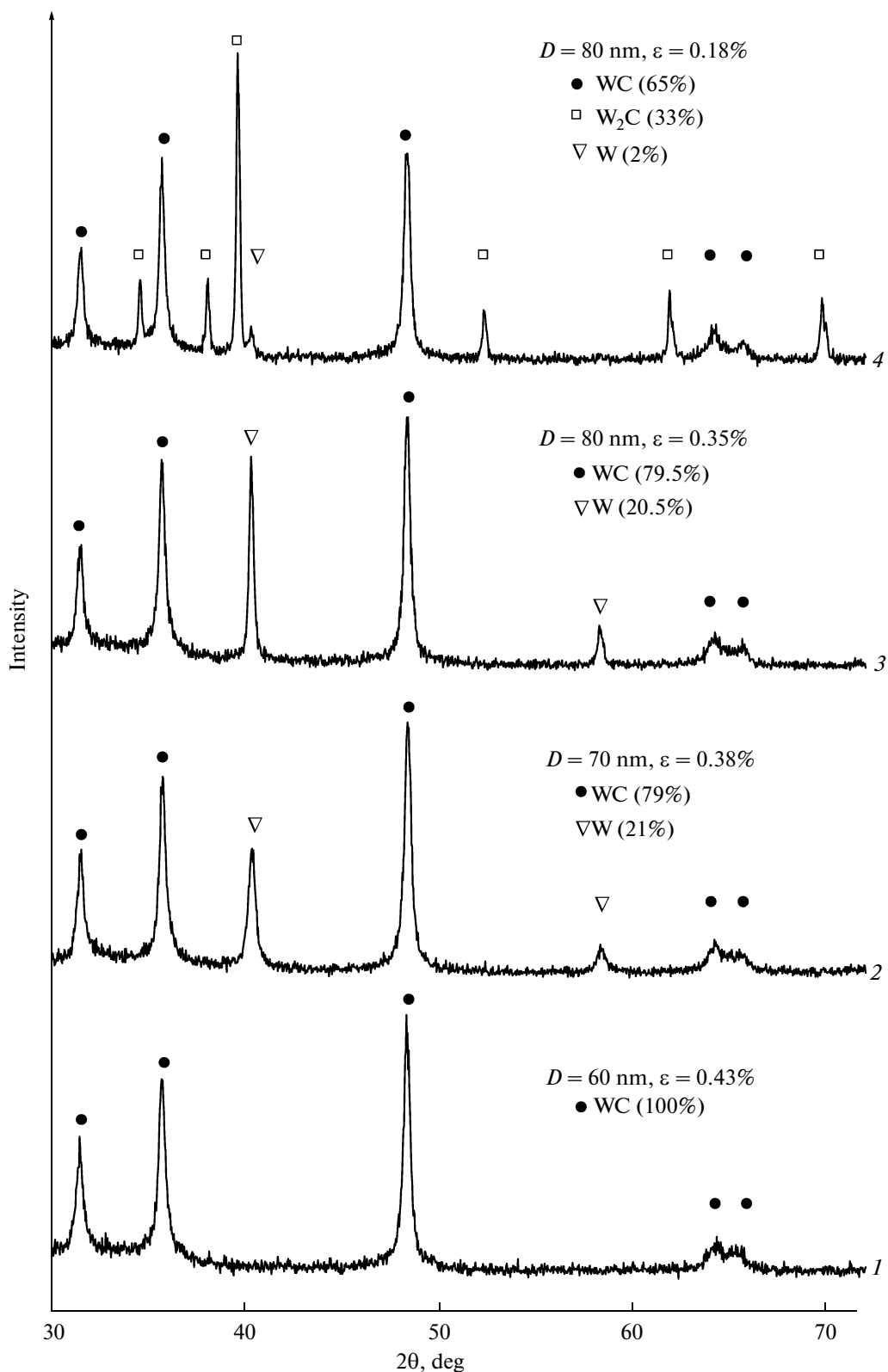


Fig. 6. XRD patterns of the WC(plasma) nanopowder (prepared by plasma synthesis) (1) before and (2–4) after vacuum annealing at (2) 800, (3) 1200, and (4) 1400°C.

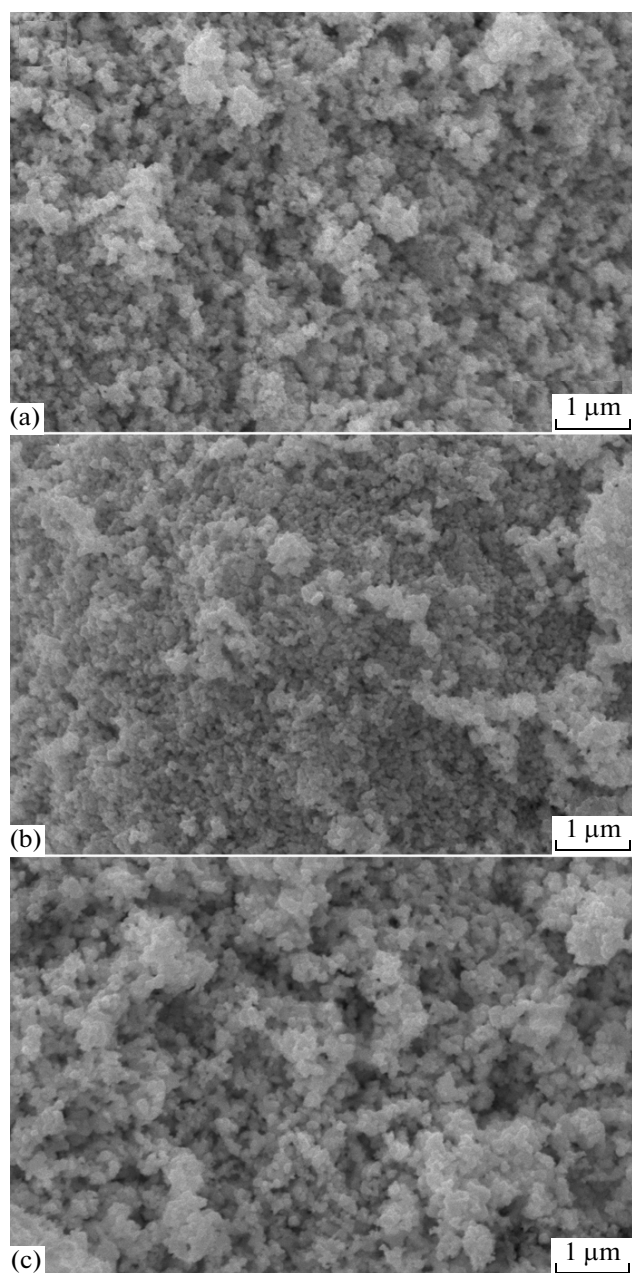


Fig. 7. SEM micrographs of the WC(plasma) nanopowder vacuum-annealed at (a) 800, (b) 1200, and (c) 1400°C.

perature at which hard alloys are commonly sintered—no well-defined coalescence (agglomeration, association, or fusion) of the nanoparticles was detected. This points to their poor sinterability, which may have an adverse effect on the quality of hard alloys.

Causes of the decarburization of the WC powders.

The present experimental data demonstrate that vacuum annealing leads to decarburization of the WC powders studied, especially in the case of the WC nanopowders and $t_{\text{ann}} \geq 800^\circ\text{C}$. The decarburization, in turn, leads to variations in the phase composition of

the powder with t_{ann} (table), which can be understood in terms of the specific features of the W–C phase diagram [13]. As shown earlier [13, 14], the lower tungsten carbide W_2C forms at $t \geq 1250^\circ\text{C}$, but the XRD pattern of the WC(mill) powder annealed at 1200°C shows reflections from W_2C . Annealing the WC(micro) powder at 1200°C also increased the percentage of W_2C , along with the formation of metallic tungsten. According to the phase diagram of the W–C system [13], such changes in phase composition can only be caused by partial decarburization of the WC powders, as observed in our experiments.

Even though similar in particle size, the WC(mill) and WC(plasma) nanopowders differed in some respects, which showed up in our annealing experiments. With increasing t_{ann} , the particle size of the WC(mill) nanopowder increases and its lattice strain decreases considerably more rapidly than those of the WC(plasma) powder. The same refers to phase transformations. In the WC(mill) powder, W_2C was present even after annealing at 1200°C and metallic tungsten disappeared upon annealing at 1400°C . The WC(plasma) nanopowder contained no W_2C after annealing at 1200°C , whereas a small amount of tungsten persisted even after annealing at 1400°C .

It is known that, during vacuum evaporation, WC loses predominantly carbon and passes into the W + WC or W_2C + WC two-phase region, depending on the evaporation temperature [15–18]. The carbon partial pressure over tungsten carbide is low even at high temperatures (1730 – 2130°C): $\approx 3.7 \times 10^{-6}$ to $\approx 4.2 \times 10^{-3}$ Pa [15, 17]. The rate of carbon vaporization, v_{C} , from tungsten carbide at 1983°C is as low as 9.24×10^{-9} g/(cm² s) [15]. According to Bolgar et al. [16], the vaporization rate in the temperature range 1975 – 2650°C (2248 – 2923 K) can be represented in the form $\log v_{\text{C}} = 6.317 - 34310/T$. For $t \leq 1400^\circ\text{C}$, the rate of carbon vaporization from WC is hundreds of thousands of times lower than v_{C} at $\approx 2000^\circ\text{C}$ and cannot account for even a hundredth of the experimentally observed carbon loss, ΔC_{C} , during vacuum annealing of WC. Thus, the observed decrease in carbon content as a result of the vacuum annealing of WC at $t_{\text{ann}} \leq 1400^\circ\text{C}$ cannot be accounted for by direct carbon vaporization.

A more likely cause of the decrease in carbon content during vacuum annealing of the WC nanopowders is oxygen impurities. Even the first nanocrystalline carbide studied, vanadium carbide nanopowder, was found to contain 5 wt % oxygen [19]. Most of the oxygen was present in the surface oxide film and adsorbed water. Krasovskii et al. [20] studied plasma-synthesized WC nanopowder and showed it to contain ≈ 2 wt % oxygen. More than 80% of the oxygen was present in X-ray amorphous tungsten oxide phases, and the rest, in water and in adsorbed form. According to Warren et al. [21] and Brillo et al. [22], the surface layer of WC in an oxygen-containing atmo-

sphere is similar in electronic structure to WO_3 . As shown in a study of the interaction of oxygen with the (0001) surface of a WC single crystal by Auger electron spectroscopy [22], oxygen chemisorption under high vacuum leads to the formation of surface tungsten oxycarbides, WO , and WO_3 .

According to previous results [21–23], heat treatment of WC nanopowder at temperatures from 900 to 1100°C removes at least 80% of the oxygen in the form of CO. Clearly, the removal of O in the form of CO reduces the carbon content of the WC powder as well. In metal and metal carbide nanopowders, oxygen is present predominantly on the surface of the particles [3, 19–24], so the oxygen content is proportional to the specific surface area S of the powder. Since the carbon loss ΔC_C during vacuum annealing is proportional to the oxygen content of the powder, C_O , it should also be proportional to the initial S of the powder.

From the unit-cell parameters of the hexagonal carbide WC (sp. gr. $P\bar{6}m2$), we find that the surface density of W atoms, n_s , is $\approx 1.4 \times 10^{19} \text{ m}^{-2}$. Therefore, when a WO_3 monolayer is formed on WC, the weight of surface oxygen per square meter of the surface is $3n_s m_a A_O$, where $m_a = 1.66 \times 10^{-24} \text{ g}$ is the atomic mass unit and A_O is the atomic weight of O. If the surface of particles is covered with p monolayers of the oxide phase, the relative oxygen content of the powder (with a specific surface area S) is to a first approximation given by

$$C_O = 3pn_s m_a A_O S = 0.00111pS. \quad (1)$$

The number of monolayers of the oxide phase is then

$$p = C_O / (3n_s m_a A_O S) = C_O / (0.00111S). \quad (2)$$

The specific surface area S of the as-prepared WC(mill) and WC(plasma) powders is 19.2 and 6.4 m^2/g , respectively (table), and C_O is 0.0152 and 0.0180 (1.52 and 1.80 wt%) as determined by EDX analysis. Therefore, the number of monolayers of the oxide phase, p , on the surface of the as-prepared WC(mill) and WC(plasma) powders is ≈ 0.7 and ≈ 2.5 . This agrees well with the report by Brillo et al. [22] that the oxide film on WC ranges in thickness from 0.6 to 2.8 monolayers.

Heating causes the oxygen to desorb from WC in the form of CO [20–22]. Therefore, the relative carbon loss is proportional to C_O :

$$\Delta C_C = (A_C/A_O)C_O = 3pn_s m_a A_C S = 0.00083pS. \quad (3)$$

From (3) and the above values $p = 0.7$ and $p = 2.5$, the expected carbon loss, ΔC_C , of the as-prepared WC(mill) and WC(plasma) nanopowders is 0.011 and 0.013 (1.1 and 1.3 wt %), respectively. Given the uncertainty in the O and C contents and the approximate character of the above estimates, the ΔC_C values obtained are in reasonable agreement with the maximum carbon loss of the WC(mill) and WC(plasma)

powders, 1.4 and 1.5 wt %, found after annealing at 1400°C.

CONCLUSIONS

Vacuum annealing of nanocrystalline WC powders at $t_{\text{ann}} \leq 1400^\circ\text{C}$ is accompanied by a marked decrease in carbon content, changes in phase composition, and an increase in particle size due to coalescence of aggregated nanoparticles. In addition, annealing reduces the lattice strain of such powders. Phase purity of WC nanopowder can be maintained during annealing by adding an excess of free carbon, but annealing is then accompanied by significant particle growth.

Vacuum annealing of microcrystalline WC powder at $t_{\text{ann}} \leq 1400^\circ\text{C}$ leads to a very small decrease in carbon content, because free carbon disappears, and has little effect on the phase composition of the powder.

ACKNOWLEDGMENTS

We are grateful to V.A. Moldaver[†] for supplying the plasma-synthesized WC powder.

This work was supported by the Russian Foundation for Basic Research (grant nos. 10-03-00023a and 12-08-00016a), the Presidium of the Russian Academy of Sciences (project no. 12-P-234-2003: Synthesis and Stabilization of Hybrid Nanoparticles for Various Applications; program no. 21: Fundamental Issues in the Development of Nanotechnologies and Nanomaterials), and the Presidium of the Ural Branch of the Russian Academy of Sciences (project no. 11-3-NP-290).

REFERENCES

1. Klyachko, L.I., Fal'kovskii, V.A., and Khokhlov, A.M., *Tverdye splavy na osnove karbida vol'frama s tonkodispersnoi strukturoi* (Fine-Grained Tungsten Carbide Based Hard Alloys), Moscow: Ruda i Metally, 1999.
2. Kurlov, A.S. and Rempel, A.A., Effect of WC Nanoparticle Size on the Sintering Temperature, Density, and Microhardness of WC–8 wt % Co Alloys, *Inorg. Mater.*, 2009, vol. 45, no. 4, pp. 380–385.
3. Gusev, A.I., *Nanomaterialy, nanostruktury, nanotekhnologii* (Nanomaterials, Nanostructures, and Nanotechnologies), Moscow: Fizmatlit, 2007, 2nd ed.
4. Rempel, A.A., Nanostructured Materials: Nanotechnologies, Properties, and Applications, *Usp. Khim.*, 2007, vol. 76, no. 5, pp. 474–500.
5. Kurlov, A.S. and Gusev, A.I., Model for Milling of Powders, *Tech. Phys.*, 2011, vol. 56, no. 7, pp. 975–980.
6. Tsvetkov, Yu.V. and Panfilov, S.A., *Nizkotemperaturnaya plazma v protsessakh vosstanovleniya* (Low-Temperature Plasma in Chemical Reduction Processes), Moscow: Nauka, 1980.
7. Kurlov, A.S. and Gusev, A.I., Particle Size Effects on the Oxidation of Tungsten Carbide Nanopowders,

[†]Deceased.

- Russ. J. Phys. Chem. A*, 2010, vol. 84, no. 12, pp. 2095–2101.
8. Kurlov, A.S. and Gusev, A.I., Effect of Particle Size on the Oxidation of WC Powders during Heating, *Inorg. Mater.*, 2011, vol. 47, no. 2, pp. 133–138.
 9. Gusev, A.I. and Kurlov, A.S., Production of Nanocrystalline Powders by High-Energy Ball Milling: Model and Experiment, *Nanotechnology*, 2008, vol. 19, no. 26, paper 265 302.
 10. Kurlov, A.S. and Gusev, A.I., Production of Nanocrystalline Powder of WC via Ball-Milling, *17th Plansee Seminar/Int. Conf. on High Performance P/M Materials*, Sigl, L.S. et al., Eds., Reutte: Plansee Group, 2009, vol. 3, pp. GT24/1–GT24/11.
 11. Kurlov, A.S. and Gusev, A.I., Determination of the Particle Sizes, Microstresses, and Degree of Inhomogeneity in Nanostructured Materials from X-Ray Diffraction Data, *Glass Phys. Chem.*, 2007, vol. 33, no. 3, pp. 276–282.
 12. Gusev, A.I. and Kurlov, A.S., Particle (Grain) Size Characterization of Nanocrystalline Materials, *Metallofiz. Noveishie Tekhnol.*, 2008, vol. 30, no. 5, pp. 679–694.
 13. Kurlov, A.S. and Gusev, A.I., Phase Equilibria in the W–C System and Tungsten Carbides, *Usp. Khim.*, 2006, vol. 75, no. 7, pp. 687–708.
 14. Kurlov, A.S. and Gusev, A.I., Tungsten Carbides and W–C Phase Diagram, *Inorg. Mater.*, 2006, vol. 42, no. 2, pp. 121–127.
 15. Hoch, M., Blackburn, P.E., Dingley, D.P., and Johnston, H.L., The Heat of Sublimation of Carbon, *J. Phys. Chem.*, 1955, vol. 59, no. 2, pp. 97–99.
 16. Bolgar, A.S., Turchanin, A.G., and Fesenko, V.V., *Termodinamicheskie svoistva karbidov* (Thermodynamic Properties of Carbides), Kiev: Naukova Dumka, 1973, pp. 97–99.
 17. Kulikov, I.S., *Termodinamika karbidov i nitridov* (Thermodynamics of Carbides and Nitrides), Chelyabinsk: Metallurgiya, 1988.
 18. *Svoistva, poluchenie i primenenie tugoplavkikh soedinenii. Spravochnik* (Properties, Preparation, and Application of Refractory Compounds: A Handbook), Kosolapova, T.Ya., Ed., Moscow: Metallurgiya, 1986.
 19. Rempel', A.A. and Gusev, A.I., Nanostructure and Atomic Order in Vanadium Carbide, *Pis'ma Zh. Eksp. Teor. Fiz.*, 1999, vol. 69, no. 6, pp. 436–442.
 20. Krasovskii, P.V., Blagoveshchenskii, Yu.V., and Grigorievich, K.V., Determination of Oxygen in W–C–Co Nanopowders, *Inorg. Mater.*, 2008, vol. 44, no. 9, pp. 954–959.
 21. Warren, A., Nylund, A., and Olefjord, I., Oxidation of Tungsten and Tungsten Carbide in Dry and Humid Atmosphere, *Int. J. Refract. Met. Hard Mater.*, 1996, vol. 14, nos. 5–6, pp. 345–353.
 22. Brillo, J., Kuhlbeck, H., and Freund, H.-J., Interaction of O₂ with WC (0001), *Surf. Sci.*, 1998, vol. 409, pp. 199–206.
 23. Ribeiro, F.H., Dalla Betta, R.A., Guskey, G.J., and Boudart, M., Preparation and Surface Composition of Tungsten Carbide Powders with High Specific Surface Area, *Chem. Mater.*, 1991, vol. 3, no. 5, pp. 805–812.
 24. Levinskii, Yu.V., Blagoveshchenskii, Yu.V., Vol'dman, G.M., and Mel'nik, Yu.I., A Mechanism of Niobium, Molybdenum, and Tungsten Nanoparticle Growth during Annealing in Vacuum and Hydrogen, *Materialovedenie*, 2006, no. 10, pp. 38–47.